Journal of Nuclear Materials 401 (2010) 98–103

Contents lists available at ScienceDirect

Journal of Nuclear Materials

journal homepage: www.elsevier.com/locate/jnucmat

FCCI barrier performance of electroplated Cr for metallic fuel

Seong Woo Yang *, Ho Jin Ryu, Jun Hwan Kim, Byoung Oon Lee, Chan Bock Lee

Recycled Fuel Development Division, Korea Atomic Energy Research Institute, 150 Deokjin-dong, Yuseong-gu, Daejeon 305-353, Republic of Korea

ARTICLE INFO

Article history:
Received 6 October 2009
Accepted 11 April 2010

ABSTRACT

As the fuel-cladding chemical interaction (FCCI) between metallic fuel and cladding material can occur at a relatively low temperature, electroplating of Cr as an FCCI barrier on the inner wall of the cladding was proposed. U–10 wt.%Zr and HT9 disks were used as fuel and cladding material to conduct diffusion couple annealing tests at 740 and 800 °C. Two kinds of Cr layers dependent on the temperature of plating bath were electroplated on the surface of the HT9 disks. The Cr layer of 20 μm in thickness, after being electroplated at a bath temperature of 50 °C and a current density of 35 A/dm^2 for 1 h, had some cracks and a small-grained structure. However, the Cr layer plated at a bath temperature of 80 °C and a current density of 56 A/dm^2 for 2 h showed a dense structure. Both Cr layers inhibited the interaction between U–10 wt.%Zr and HT9 at a relatively high annealing temperature. U penetrated into the Cr layer plated at a bath temperature of 50 °C due to its penetrable structure. The Cr layer plated at a bath temperature of 80 °C showed a better performance than the Cr layer plated at a bath temperature of 50 °C as a diffusion barrier material with less U penetration.

1. Introduction

A sodium-cooled fast reactor (SFR) has been developed to use fissionable materials efficiently and to reduce the volume of high-level radioactive elements. Alloys of uranium, zirconium, and transuranic elements (TRUs) extracted from the spent fuel of pressurized water reactors (PWRs) were considered used in an SFR as metallic fuel material [1]. However, metallic alloys containing U, minor actinides, and fission products can chemically interact with the elements of ferritic/martensitic steel (FMS), which is the candidate material for cladding, at a relatively low temperature. It has been called the fuel-cladding chemical interaction (FCCI), and it deteriorates the performance and integrity of the fuel and cladding. It is reported that the eutectic melting between U–Pu–Zr and Fe occurs above 650 °C [2]. To guarantee the performance of the fuel and cladding, it is necessary to prevent the inter-diffusion of the elements in the fuel and cladding materials.

To interrupt such FCCI phenomena, some researchers proposed the insertion of an FCCI barrier between the fuel and cladding. They conducted the annealing tests with barrier materials to observe their performance [3–6]. Keiser and Cole used the V and Zr disks and observed their barrier performance [3]. Crawford et al. fabricated Zr-sheathed U–Zr metallic fuel and irradiated the fuel in an EBR-II reactor up to 2 at.% of burn-up [4]. Tokiwai et al. formed the ZrN layer on HT9 and used a V foil to reduce chemical inter-diffusion [5]. Previous studies on the FCCI barrier have focused mainly on V and Zr of the liner-type. Although the FCCI barrier of the liner-type showed a good performance, it is expected that the application on actual claddings may be difficult because it is hard to put a thin barrier layer on the inner surface of cladding tubes uniformly. A recent evaluation of the thin foils of some candidate elements showed that not only V but also Cr showed an excellent FCCI barrier performance [6]. Cr can be easily coated on the surface of the cladding by the electrolytic plating method. For example, Cr was electroplated on the inner surface of gun barrels in order to increase its duty life [7].

In this study, Cr electroplating on the cladding surface is proposed as an FCCI barrier due to its advantages in diffusion barrier performance and manufacturing feasibility based on previous researches. The optimum condition of Cr electroplating on the surface of HT9 was established. The FCCI barrier performance of electroplated Cr layers was evaluated by diffusion couple annealing tests.

2. Experimental methods

2.1. Specimen

U–10 wt.%Zr and HT9 (Fe–12.0Cr–1.0Mo–0.6Ni–0.6Mn–0.52W–0.3V, etc. all values are wt.%) disks were used as fuel and cladding material to conduct diffusion couple annealing tests. U–10 wt.%Zr was fabricated by an induction melting of elemental lumps of U and Zr. A cast rod with a diameter of 6 mm was cut into disks with a 1 mm thickness. The diameter and thickness of the HT9 disks were 8 and 1.5 mm, respectively.

* Corresponding author. Tel.: +82 42 868 2511; fax: +82 42 868 8990.
E-mail address: swyang@kaeri.re.kr (S.W. Yang).

0022-3115/$ - see front matter © 2010 Elsevier B.V. All rights reserved.
doi:10.1016/j.jnucmat.2010.04.004

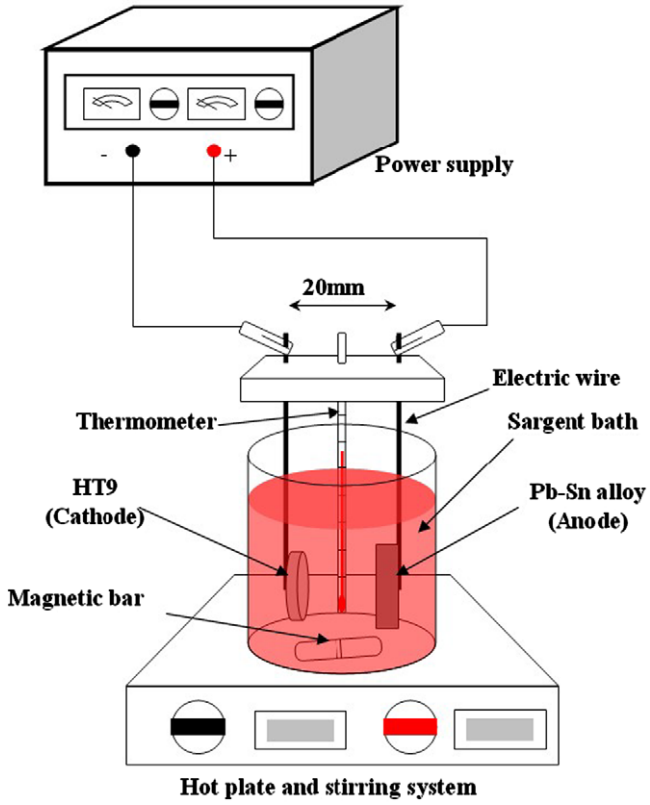

Fig. 1. A schematic illustration of a Cr-electroplating apparatus.

2.2. Cr electroplating on the surface of HT9 disks

Before the electroplating, the HT9 disks were polished with fine SiC paper, pickled, and cleaned. The scheme of the electroplating apparatus composed of plating bath, a power supply, a thermometer, a stirring and heating system, and etc. is shown in Fig. 1. A Sargent bath containing 250 g/l of chromic acid (CrO_3) and 2.5 g/l of sulfuric acid (H_2SO_4) was used as an electrolyte. During the electroplating, the electrolyte was maintained with a isothermal condition and stirred by a magnetic bar. A Pb–Sn alloy was used as the anode metal. A pure Cr layer was electroplated on the surface of HT9, as shown in the study by Kim et al. [8] Two methods for Cr electroplating dependent on a bath temperature were used. The Cr layer plated at a bath temperature of 50 °C was conventionally called 'hard Cr', and it has been applied in various industries because of its strong mechanical properties [9–10]. However, it has many cracks which can

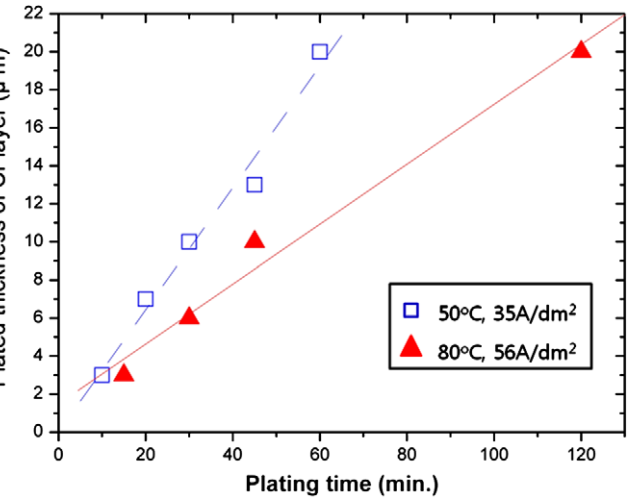

Fig. 2. The electroplated Cr thickness with the plating time at bath temperatures of 50 °C and 80 °C.

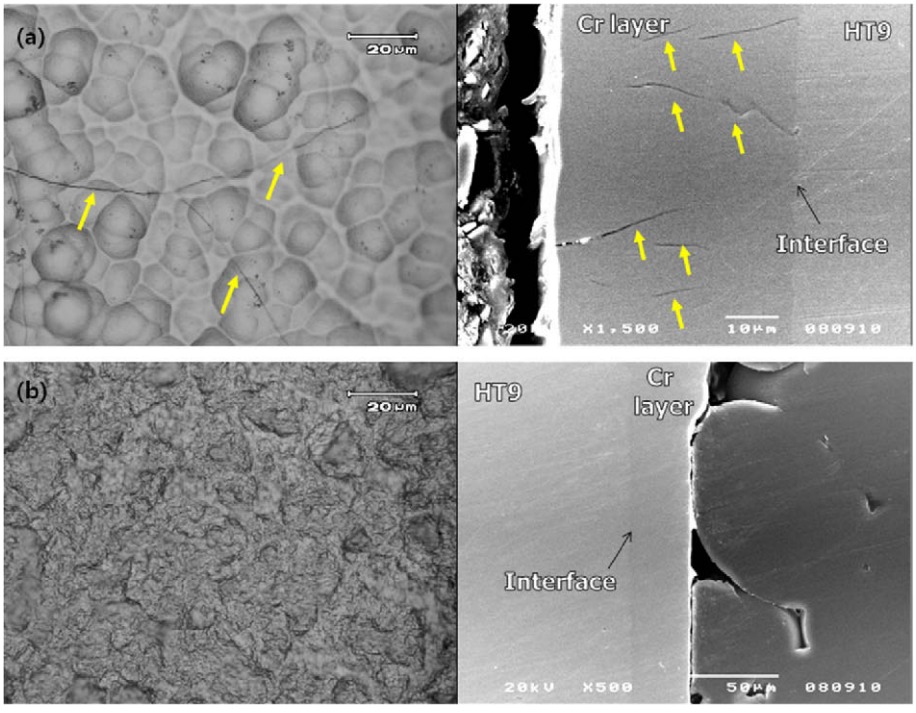

Fig. 3. The surface morphology and cross-sectional image of: (a) a Cr layer plated at a bath temperature of 50 °C and (b) a Cr layer plated at a bath temperature of 80 °C: Cracks were observed in the Cr layer plated under a bath temperature of 50 °C. (Yellow arrows). (For interpretation of the references to colour in this figure legend, the reader is referred to the web version of this article.)

deteriorate corrosion resistance. Sohi et al. studied a Cr plating method to improve the corrosion resistance of Cr layer [11]. In his study, only changing bath temperature up to 80 °C could form a Cr layer which has a low crack density. At the Cr plating at a bath temperature of 80 °C, a higher current density was needed than the Cr plating at a bath temperature of 50 °C due to the drop of current efficiency according to the increase in plating temperature. Fig. 2 shows the thickness of the Cr layer plated at bath temperatures of 50 °C and 80 °C with the plating time. The thickness of the Cr layer was linearly increased according to the increase of plating time. To form a Cr layer with a thickness of 20 μm at a bath temperature of 50 °C, a current density of 35 A/dm^2 for 1 h was necessary. However, 56 A/dm^2 for 2 h was needed to form the 20-μm Cr layer at a bath temperature of 80 °C. Fig. 3 shows the surface morphology and cross-sectional image of both electroplated Cr layers on the surfaces of the HT9 disks. Some cracks and a small-grained structure were observed in the Cr layer plated at a bath temperature of 50 °C, as shown in Fig. 3a. However, cracks were not observed, and the dense structure was formed in the Cr layer plated at a bath temperature of 80 °C, as shown in Fig. 3b.

2.3. Diffusion couple annealing test

After the electroplating, the sample was cleaned and used for the annealing tests with U–10 wt.%Zr. Before the annealing test, U–10 wt.%Zr was polished with fine SiC paper. Fig. 4. shows the scheme of the diffusion couple. Both sides of the diffusion couple were composed of stainless steel screw bolts that made it possible to tighten both U–10 wt.%Zr and Cr-plated HT9 with a proper force in a stainless steel clamp tube. The test specimen was wrapped in Ta foil to prevent a reaction with the clamp wall and bolts. The diffusion couple tests were conducted in a vacuum tube furnace under annealing temperatures of 740 and 800 °C. During the test, the inside of the furnace was maintained under a vacuum of $10^{-3}\sim10^{-4}$ kPa. After the tests, the diffusion couple was water-quenched to room temperature. Recovered specimens were cut, mounted, and polished in order to observe the cross-sectional interface between U–10 wt.%Zr and the Cr-plated HT9. A scanning electron microscope (SEM) and an energy dispersive X-ray spectroscopy (EDS) were used to observe the inter-diffusion of constituent elements.

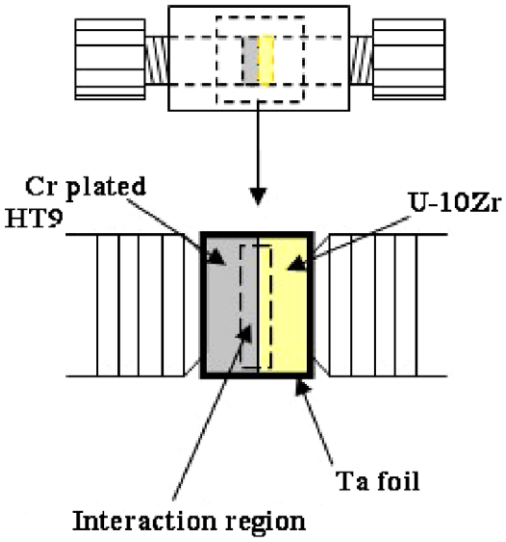

Fig. 4. A schematic illustration of a diffusion couple clamp set.

3. Results and discussion

Some researchers have investigated the chemical interactions between U–Zr–X and Fe-base materials without an FCCI barrier [12–16]. As a result of their studies, active interactions were observed in the diffusion couple samples at annealing temperatures above 700 °C. Both elements of U and Fe mainly reacted with each other and formed intermetallic compounds. At an annealing temperature above 725 °C, liquid phases by eutectic meting were formed at the interface region of the diffusion couple samples between U–Zr and FMS [6].

Fig. 5 shows the back-scattered electron images of annealed samples between U–10 wt.%Zr and HT9 without an FCCI barrier at the annealing temperatures of 740 and 800 °C. Table 1 shows

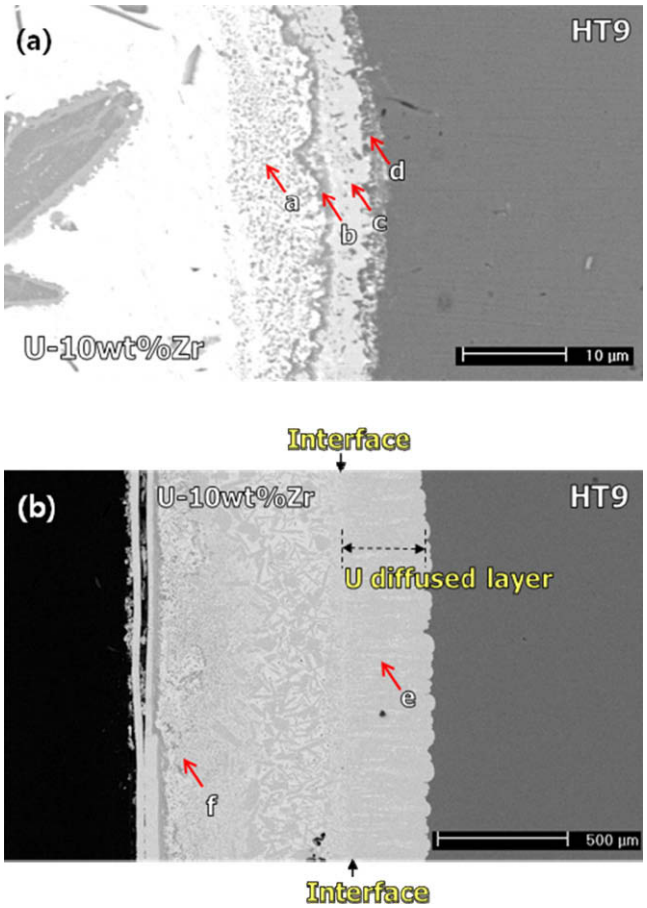

Fig. 5. Back-scattered electron images of annealed samples between U–10 wt.%Zr and HT9 without a barrier at: (a) 740 °C for 96 h and (b) 800 °C for 25 h.

Table 1
Element content of the annealed sample between U–10 wt.%Zr and HT9 without a barrier: selected points (red arrows) in Fig. 5. (For interpretation of the references to colour in this Table 1 legend, the reader is referred to the web version of this article.)

Annealing condition	Location	Element (at.%)	Phase
740 °C, 96 h	a	58Zr–42U	Zr-rich
	b	80Zr–15U–5Fe	Zr-rich
	c	65Fe–32U–3Cr	UFe_2
	d	52Fe–42Cr–8U	Cr-rich
800 °C, 25 h	e	58Fe–26U–13Cr–3Zr	UFe_2
	f	54Fe–25Zr–16Cr–3U–2Ta	Eutectic melted

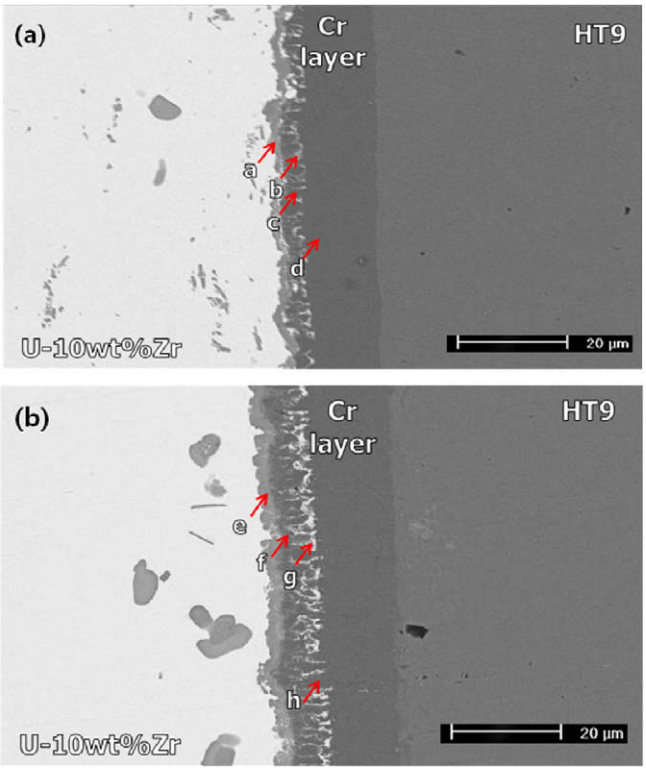

Fig. 6. Back-scattered electron images of annealed samples between U–10 wt.%Zr and Cr-plated HT9 under a bath temperature of 50 °C at annealing temperatures of: (a) 740 °C for 96 h and (b) 800 °C for 48 h. (For interpretation of the references to colour in this figure legend, the reader is referred to the web version of this article.)

Table 2
Element content of the annealed sample between U–10 wt.%Zr and Cr-plated HT9 under a bath temperature of 50 °C: selected points (red arrows) in Fig. 6.

Annealing condition	Location	Element (at.%)	Phase
740 °C, 96 h	a	88Zr–7U–5Cr	Zr-rich
	b	91Cr–9U	U-rich
	c	99Cr–1U	Pure Cr
	d	100Cr	Pure Cr
800 °C, 48 h	e	70Cr–28Zr–2U	Cr–Zr intermediate
	f	99Cr–0.5U–0.5Zr	Pure Cr
	g	79Zr–21U	U-rich
	h	99Cr–1U	Pure Cr

the element content of selected points in the annealed samples that were indicated in Fig. 5, where the FCCI actively occurred. As shown in Fig. 5 and Table 1, an interaction layer composed of the Zr-rich layer, UFe_2, and the Cr-rich layer was observed in the annealed sample at 740 °C for 96 h. The eutectic-melted structure was observed in the annealed sample at 800 °C for 25 h. U diffused into HT9 at about 200 μm and formed UFe_2. Fe and Cr were detected in the region far from the interface.

Fig. 6 shows the back-scattered electron images of annealed samples between U–10 wt.%Zr and the Cr-coated HT9 that was plated at a bath temperature of 50 °C. The tests were conducted under annealing temperatures of 740 °C for 96 h and 800 °C for 48 h. Table 2 shows the element content of selected points in the annealed samples that are indicated in Fig. 6. The eutectic-melted structure or intermetallic phases by the interaction between U and Fe were not observed in spite of the high annealing temperatures. However, an EDS analysis revealed that the penetrating phase containing U was observed about 5–8 μm. U was only detected in the bright-penetrating phase, not in any region inside the Cr layer. U penetrated through the low density region of the Cr layer that is cracks and grain boundaries. The penetrating depth was longer in the annealed samples at 800 °C than 740 °C when compared with the results of the diffusion couple samples, as shown in Fig. 6a and b.

Although Zr could not be observed in the penetrating phases and the Cr layer, the Zr–Cr–U compounds were observed at the interface of U–10 wt.%Zr and the Cr layer. A Zr-rich layer containing a small amount of Cr and U (88 at.%Zr–7 at.%U–5 at.%Cr) was observed in the annealed sample at 740 °C, as shown in Fig. 6a. However, the Cr content increased when the annealing temperature increased to 800 °C. 70 at.%Cr compound layers were observed in the annealed samples at 800 °C for 48 h, as shown in Fig. 6b. Only a small amount of U was contained in the Zr–Cr–U compound. It seems that the Zr-rich phase at the interface and the Cr layer reacted to form $ZrCr_2$-based intermetallic compounds at 800 °C.

The penetration of U-containing phases into the Cr layer is shown clearly in Fig. 7, which is the back-scattered electron image of an annealed sample at 800 °C for 25 h between U–10 wt.%Zr and the Cr-coated HT9 that was plated at a bath temperature of 50 °C. Some penetrating phases were reached at the region of HT9 through the Cr layer. However, most of the penetrating phases were penetrated up to a similar depth of about 7–8 μm. The former one was caused by the cracks in the Cr layer. The cracks in the Cr layer provided a straight penetrating path. The latter one was caused by the grain boundaries in the Cr layer, which formed something similar to a network structure.

Fig. 8 shows the back-scattered electron and element-mapping images using the annealed sample at 800 °C for 48 h. In the fuel region between U–10 wt.%Zr, Zr-rich phases were observed, as shown in Fig. 8b. The intermetallic phase of Zr–Cr was observed in the interface. Diffusion of Cr to the fuel region was not observed, as shown in Fig. 8c. U penetrated into the Cr layer, as shown in Fig. 8d. A great portion of penetrated U was located at the end of the penetrating phase. Fe could not be detected in the Cr layer and fuel region, as shown in Fig. 8e.

Fig. 9 shows the back-scattered electron images of diffusion couple samples of U–10 wt.%Zr and the Cr-coated HT9 that was plated at a bath temperature of 80 °C. Those samples were annealed at 800 °C for 25 and 48 h. Table 3 shows the element content of selected points in the annealed samples that were indicated in Fig. 9. Although penetrating phases of about 7–8 μm were observed in the samples, they were remarkably reduced when compared with the results of the diffusion couple samples containing the Cr layer plated at a bath temperature of 50 °C, as shown in Figs. 6 and 7. Both Cr layers dependent on a bath temperature showed similar interaction behavior at the interface, which was the intermediate phase of the Cr–Zr interaction. The Cr layer plated at a bath temperature of 80 °C seemed to have a relatively

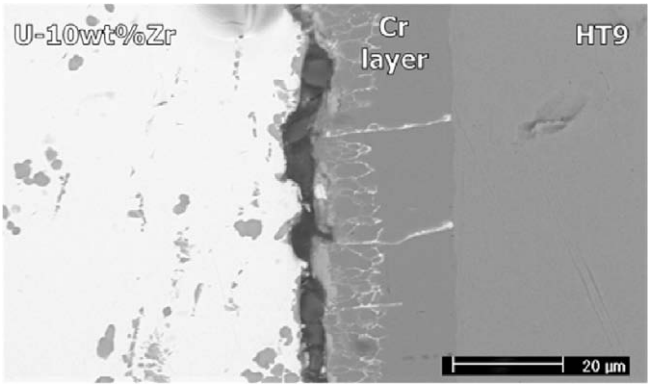

Fig. 7. Back-scattered electron image of an annealed sample between U–10 wt.%Zr and Cr-plated HT9 under a bath temperature of 50 °C at 800 °C for 25 h.

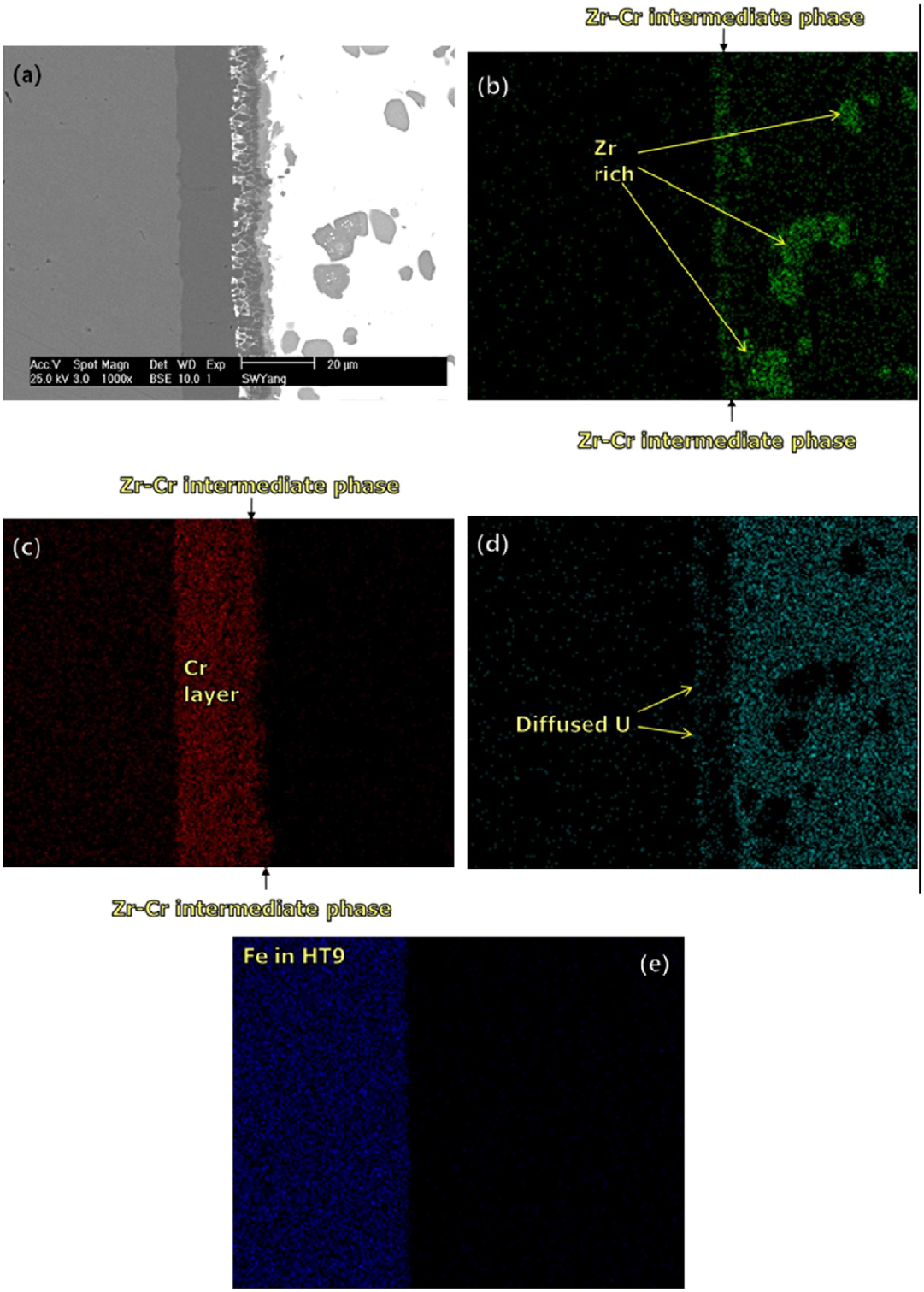

Fig. 8. Back-scattered electron and element-mapping images of an annealed sample at an annealing temperature of 800 °C for 48 h: (a) back-scattered electron image, (b) green: Zr, (c) red: Cr, (d) jade: U, and (e) blue: Fe. (For interpretation of the references to colour in this figure legend, the reader is referred to the web version of this article.)

better FCCI barrier performance than the Cr layer plated at a bath temperature of 50 °C due to the crack-free and large-grained structure.

According to the binary phase diagram of U–Cr, U dissolves up to only 4 at.% in Cr at around 800 °C. The interaction between U and Cr was not observed in the annealed samples, and the Cr–Zr interaction was the main reaction at the interface. In the binary Cr–Zr system, the $ZrCr_2$ Laves phase exists as an intermediate phase at temperatures of 740–800 °C [17]. U content in the $ZrCr_2$ phase is not higher than 5 at.%, and further penetration of U into the cracks and boundaries in the Cr layer might be hindered once the $ZrCr_2$ layer is formed on the Cr layer. Therefore, the penetrating depth was similar at the annealing temperature of 800 °C that was independent of the annealing time.

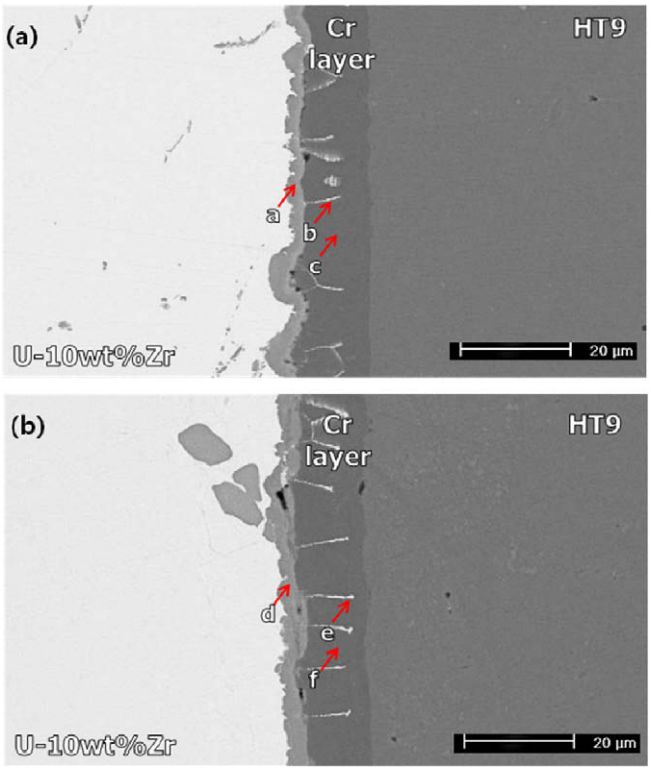

Fig. 9. Back-scattered electron image of an annealed sample between U–10 wt.%Zr and Cr-plated HT9 under a bath temperature of 80 °C at an annealing temperature of 800 °C for: (a) 25 and (b) 48 h.(For interpretation of the references to colour in this figure legend, the reader is referred to the web version of this article.)

Table 3
Element content of the annealed sample between U–10 wt.%Zr and Cr-plated HT9 under a bath temperature of 80 °C: selected points (red arrows) in Fig. 9.

Annealing condition	Location	Element (at.%)	Phase
800 °C, 25 h	a	65Cr–31Zr–4U	Cr–Zr intermediate
	b	80Cr–20U	U-rich
	c	100Cr	Pure Cr
800 °C, 48 h	d	69Cr–29Zr–2U	Cr–Zr intermediate
	e	78Cr–22U	U-rich
	f	100Cr	Pure Cr

The compositional profile of the constituent element across the interaction layers between U–10 wt.%Zr and the Cr layer plated at a bath temperature of 80 °C annealed at 800 °C for 25 h is presented in Fig. 10. The zero position in the horizontal axis indicates the interface between the Cr layer and HT9. Although the drop of Cr content and the elevation of Zr content were observed in a horizontal position of −13 μm due to the formation of the $ZrCr_2$ intermetallic phase in the interface between the Cr layer and U–10 wt.%Zr, any elements in U–10 wt.%Zr did not diffuse to the region of the Cr layer and HT9. Also, Fe in HT9 could not diffuse into the fuel region due to the Cr barrier.

4. Conclusion

To prevent an FCCI between metallic fuel and cladding material, electroplating of Cr as a FCCI barrier on the surface of the cladding was proposed. At a bath temperature of 50 °C, a Cr layer plated at a rate of 20 μm/h was plated on the surface of HT9 at a current

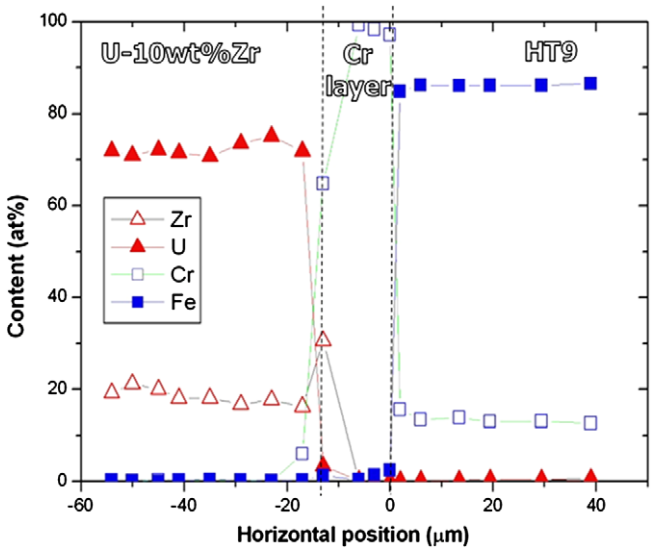

Fig. 10. The compositional variation of the constituent element across the interaction between U–10 wt.%Zr and Cr-plated HT9 under a bath temperature of 80 °C at an annealing temperature of 800 °C for 25 h: same specimen with Fig. 10a.

density of 35 A/dm^2. A current density of 56 A/dm^2 was necessary at a bath temperature of 80 °C to form the Cr layer that was plated at a rate of 10 μm/h. Some cracks and a small-grained structure were observed in the former Cr layer, but the latter one had a dense structure. Although eutectic melting in the U–10 wt.%Zr vs. HT9 diffusion couples was prevented by the plated Cr layer at 740 and 800 °C, a penetration of U into the Cr layer was observed. The Cr layer plated at a bath temperature of 80 °C showed a better performance as an FCCI barrier with less U penetration than the Cr layer plated at a bath temperature of 50 °C.

Acknowledgement

This study was supported by the National Nuclear R&D Program of the Ministry of Education, Science and Technology (MEST) of Korea.

References

[1] J.S. Cheon, S.J. Oh, B.O. Lee, C.B. Lee, J. Nucl. Mater. 385 (2009) 559.
[2] K. Nakamura, T. Ogata, M. Kuruta, T. Yokoo, M.A. Mignanelli, J. Nucl. Sci. Technol. 38 (2001) 112.
[3] D.D. Keiser, J.I. Cole, GLOBAL-2007, Boise, Idaho, September 9–13, 2007.
[4] D.C. Crawford, C.E. Lahm, H. Tsai, R.G. Pahl, J. Nucl. Mater. 204 (1993) 157.
[5] M. Tokiwai, A. Kawabe, R. Yuda, T. Usami, R.H. Nakamura, H. Yahata, J. Nucl. Sci. Technol., Supp. 3 (2002) 917.
[6] H.J. Ryu, B.O. Lee, S.J. Oh, J.H. Kim, C.B. Lee, J. Nucl. Mater. 392 (2009) 206.
[7] K.M. Yin, C.M. Wang, Surf. Coat. Technol. 114 (1999) 213.
[8] J.H. Kim, H.J. Ryu, S.W. Yang, B.O. Lee, S.J. Oh, C.B. Lee, D.H. Han, ICAPP-2009, Tokyo, Japan, May 10–14, 2009.
[9] I.K. Dennis, T.E. Such, Nickel and Chromium Plating, third ed., Woodhead Publishing, Cambridge, UK, 1993.
[10] R.F. Guffie, The Handbook of Hard Chromium Plating, Gardener Publications Inc., USA, 1986.
[11] M.H. Sohi, A.A. Kashi, S.M.M. Hadavi, J. Mater. Process. Technol. 138 (2003) 219.
[12] K. Nakamura, T. Ogata, M. Kurata, A. Itoh, M. Akabori, J. Nucl. Mater. 275 (1999) 246.
[13] T. Ogata, M. Kurata, K. Nakamura, A. Itoh, M. Akabori, J. Nucl. Mater. 250 (1997) 171.
[14] D.D. Keiser, M.C. Petri, J. Nucl. Mater. 240 (1996) 51.
[15] D.D. Keiser, M.A. Dayananda, Metall. Trans. 25A (1994) 1649.
[16] D.D. Keiser, M.A. Dayananda, J. Nucl. Mater. 200 (1993) 229.
[17] S. Kanazawa, Y. Kaneno, H. Inoue, W.Y. Kim, T. Takasugi, Intermetallics 10 (2002) 783.